USING INFRARED THERMOGRAPHY FOR ASSESSING THE FATIGUE BEHAVIOUR OF POLYMER MATRIX COMPOSITES

J. Montesano[1*], H. Bougherara[2], Z. Fawaz[1]

[1]*Dept. of Aerospace Eng., Ryerson University, 350 Victoria St., Toronto, Canada M5B2K3*
[2]*Dept. of Mechanical & Ind. Eng., Ryerson University, 350 Victoria St., Toronto, Canada M5B2K3*
**gmontesa@ryerson.ca*

Keywords: Fatigue, Polymeric Composites, Infrared Thermography, Damage Accumulation.

Abstract
The focus of this study is to assess the fatigue behaviour and the corresponding damage states of a textile polymeric composite material with the use of infrared thermography. Static results confirmed that the dominant damage mechanism is cracking in the braider yarns, which was monitored using thermographic images and confirmed by edge replication observations. Fatigue results confirmed that the saturation of braider yarn cracks during cyclic loading corresponded to changes in the stiffness degradation rate as well as the surface temperature profile. This was confirmed by edge replication and scanning electron microscopic analysis. Thermography was successful in monitoring the development of fatigue damage as well as predicting the damage states of the braided polymeric composite material.

1 Introduction

In recent years, advanced fiber-reinforced polymer matrix composite (PMC) materials have been preferred for primary load bearing aerospace applications due to their excellent mechanical properties including superior strength-to-weight and stiffness-to-weight ratios. Developing a comprehensive understanding of the material mechanical behaviour is therefore crucial to ensure the widespread application of these advanced materials. When subjected to cyclic loading composite materials can prematurely fail at loads that are significantly lower than their ultimate strengths, which can limit their service life and damage tolerance capabilities. Therefore, assessing the fatigue behaviour of composite materials by tracking damage progression and material property degradation is imperative for developing corresponding tools to predict critical damage states or the fatigue life. A number of non-destructive evaluation (NDE) techniques have been employed in the past with this aim. Some of these NDE techniques include acoustic emission [1], ultrasonic scanning [2] and x-ray tomography [3]. Recently, infrared thermography (IRT) has been established as a means to monitor the performance of composite materials [4]-[5], providing a non-contact, in-situ and a real-time assessment of these materials. It is therefore the objective of this study to utilize IRT for monitoring the development of fatigue damage in a carbon fiber-reinforced PMC material. An infrared (IR) camera is used to not only monitor the surface temperature of the cyclically loaded specimens, but to capture the crack saturation point that corresponds to the exhibited material behavior. The subsequent sections outline the experimental details, present the results with the corresponding analysis and discussion, and summarize the main conclusions.

2 Experimental details

A thermosetting polyimide resin reinforced with a tri-axially braided carbon fiber fabric (T650/35-6K) with a 0°/±θ orientation was investigated. The flat composite panels were manufactured using a resin transfer molding (RTM) technique, resulting in panels with final dimensions of 362 mm (warp) by 350 mm. Each panel was cut along the warp direction (i.e., 0° yarn direction) into 12 specimens using an abrasive waterjet cutting technique. The nominal dimensions of each specimen were 355 mm x 25 mm, and were equipped with 10° tapered aluminum end tabs to eliminate any potential issues with gripping induced failure.

All uniaxial tensile static and fatigue tests were conducted at room temperature on an MTS 322 test frame equipped with hydraulically operated wedge grips. A surface mounted extensometer was used to monitor the local axial strain and for calculation of the progressive material stiffness during the cyclic loading tests. A FLIR SC5000 infrared camera with a pixel resolution of 320 x 240 and a temperature sensitivity of <20 mK was used to monitor the test coupon surface temperature. A photograph of the test setup with application of the IR camera is shown in Figure 1. For the cyclic tests, the infrared camera was synchronized to the test controller in order to trigger the acquisition of images at the same point in each loading cycle, which was necessary to eliminate any variation of temperature due to cycling between maximum and minimum cyclic stresses [4]. In addition, edge replications were taken for some of the fatigue test coupons using acetone and cellulose acetate film to track damage progression during cyclic loading, while scanning electron microscopy (SEM) was utilized for additional damage observations *post mortem* after destructive sectioning of the specimens. The ultimate static tests were conducted in displacement control with a constant crosshead speed of 2 mm/minute. Tension-tension fatigue tests were conducted in load control using a constant amplitude sinusoidal waveform, a loading frequency of 5 Hz and a stress ratio of 0.1 at various maximum applied stress levels.

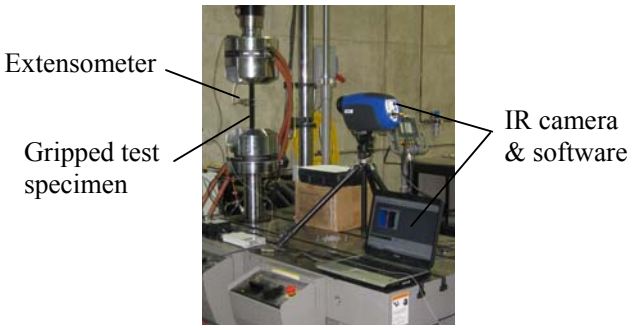

Figure 1. Photograph of experimental setup with infrared camera.

3 Experimental results

3.1 Static

A number of ultimate static test were conducted initially to define the ultimate strength of the test specimens which was required for the fatigue tests, and to investigate the microscopic damage mechanisms under quasi-static loading conditions. Edge replications were extracted for two static test specimens for the purpose of identifying the dominant damage modes and determining the evolving crack density. These tests were paused at various stress levels in a stepwise manner to extract the edge replications while the load was held constant. After pausing the tests at load levels corresponding to 7%, 14%, 21%, 35%, 42%, 50%, 57%, 75% and 85% of the ultimate strength, loading resumed with the same constant rate. The IR camera was employed for two additional static tests to continuously monitor the temperature profiles

on the material surface as loading increased. The edge replications revealed that the dominant damage mechanism was transverse cracking in the braided yarns. Braider yarn cracks were also found to be the dominant damage modes for a similar tri-axially braided composite material statically loaded in tension [6]. This was confirmed by *post mortem* SEM analysis as shown in Figure 2. Note that the 0˚ yarns are outlined for clarity in the image. There was no visible damage in the 0˚ yarns, and some localized cracking at the adjacent braider yarn interfaces. The evolution of the braider yarn cracks was continuous for the duration of the static tests, reaching a higher propagation rate and thus a higher crack density in the latter stages of quasi-static loading.

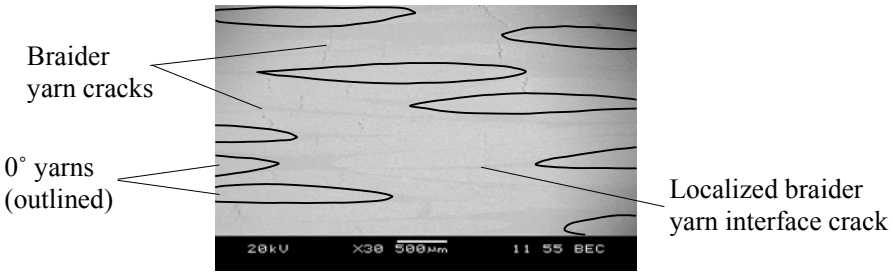

Figure 2. SEM photomicrograph of static test specimen cross-section after failure.

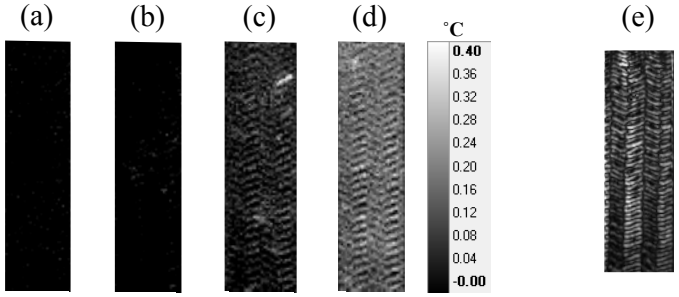

Figure 3. Real-time IR images of static test specimen at stress level of (a) 25% UTS, (b) 52% UTS, (c) 63% UTS, (d) 82% UTS, and (e) IR image acquired using lock-in thermography.

Real-time images extracted using the IR camera confirm that the saturation of braider yarn cracks is in fact much higher in the latter stages of loading, and damage is widespread throughout the specimen length. Figure 3 (a)-(d) show a series of these images for an ultimate static test specimen. The initiation of damage in the braider yarns is indicated by the sudden temperature increase in the braider yarn regions (i.e., the lighter regions in the figure) at lower stress levels. As loading progresses, the initiated cracks begin to propagate along the braider yarn directions and additional cracks continue to form, which maintain the higher temperature within the damaged braider yarns and/or causes more sudden temperature increases, respectively (see Figure 3 (c)). As the stress level approaches the ultimate, the braider yarns all show indications of cracking, which is consistent with the *post mortem* SEM observations. The IR camera has successfully captured the progressive damage states within the braider yarns. In order to more clearly illustrate the temperature variation between the braider yarns and the resin-rich zones of the specimen, an additional test was conducted using the lock-in thermographic feature of the IR camera. Lock-in thermography is useful for establishing local stress concentrations on materials, and is based on the principle of thermoelasticity [7]. To facilitate this, a test specimen was cycled at a low stress level (i.e., 30% UTS, 5 Hz, R=0.1) to obtain a constant temperature on the specimen gage section and allow the lock-in feature of the IR camera to perform. An obtained IR image of the specimen is shown in Figure 3 (e).

The high temperatures exhibited by the braider yarns are clearly regions subjected to higher local stresses when compared to the resin-rich zones between the braider yarns. This further supports the damage observations obtained through SEM and edge replication observations.

3.2 Fatigue

Fatigue tests were conducted at maximum applied stress levels in the range of 50%-80% UTS until the specimens failed. Strain data acquired using the surface mounted extensometer was used to determine the dynamic stiffness of the specimens throughout the duration of each test. The IR camera was employed for multiple tests at each applied maximum stress level to monitor the specimen surface temperature distribution at different stages in cycling. Edge replications were also extracted for some tests in an effort to track the damage progression during cycling at the different maximum applied stress levels. These tests were paused at various predetermined cyclic intervals to extract the edge replications during a zero-load dwell. After pausing the tests, loading resumed with the same fatigue loading conditions. The edge replication results for all maximum applied stress levels revealed that braider yarn cracking was the dominant damage mechanism. In addition, significantly more braider yarn interface cracks were observed when compared to the static test specimens. The edge replication results for specimens cycled at 70% and 80% UTS maximum applied stresses are shown in Figure 4 (a) and (b), respectively, as crack density profiles (i.e., the ordinate is number of cracks/mm^2). Both plots include the braider yarn crack density as well as the interface crack density. In both cases, and for all cyclic tests conducted, the braider yarn crack development is constant or very slightly increasing after an initial large increase in the number of cracks. The braider yarn crack density for the specimens shown in Figure 4 (a) and (b) reach a saturation after approximately 5,000 and 1,000 cycles, respectively. The number of interface cracks is relatively small compared to the number of braider yarn cracks. Note that the interface crack density for the 80% UTS test specimen began to decrease after approximately 4,000 cycles. This was due to the coalescence of existing local interface cracks combining to form larger cracks, resulting in a lower apparent crack count. The interface cracks did reach a saturation much earlier in cycling, for all load levels, when compared to the braider yarn cracks. After saturation, the interface cracks were found to notably increase in length and coalesce in the latter stages of cycling as indicated.

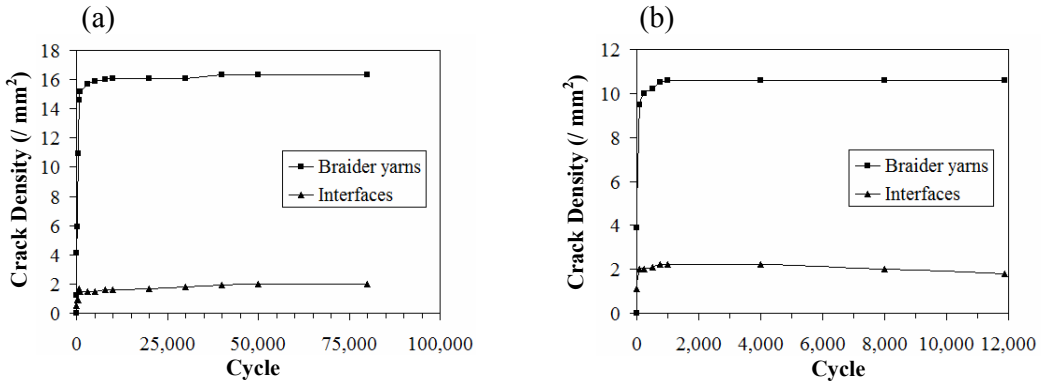

Figure 4. Crack density profiles of test specimens cycled at (a) 70% UTS, (b) 80% UTS.

The thermographic results for test specimens cycled at 70% UTS and 80% UTS maximum stress are shown in Figure 5 (a) and (b), respectively, as surface temperature-cycle plots. The temperature profiles follow a similar trend as the braider yarn crack density plots. In fact, the

saturation of the braider yarn cracks corresponds to the same cycles that the temperature plateau is attained for each stress level (see Figures 4 and 5). For all tests the interface cracks saturate prior to the braider yarn cracks, which indicates that the initial temperature rise is mainly due to braider yarn crack development and the associated local viscous matrix heating due to cycling. Figures 6 (a) and (b) show real-time IR images obtained for the 70% UTS test specimen at the indicated cyclic intervals. The images clearly reveal the higher temperature regions associated with the braider yarns (i.e., the lighter regions), which are oriented along the ±θ directions. A plot of the temperature profiles for a typical braider yarn and a resin-rich zone is shown in Figure 6 (c). Although the regions show a similar temperature profile for the duration of cyclic loading, the consistently higher temperature rise in the braider yarns compared to the resin rich regions is illustrated.

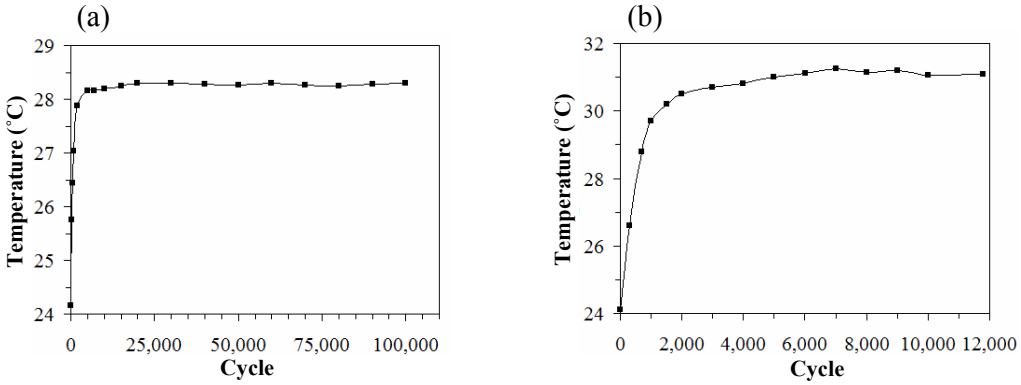

Figure 5. IRT temperature profiles for test specimens cycled at (a) 70% UTS, and (b) 80% UTS.

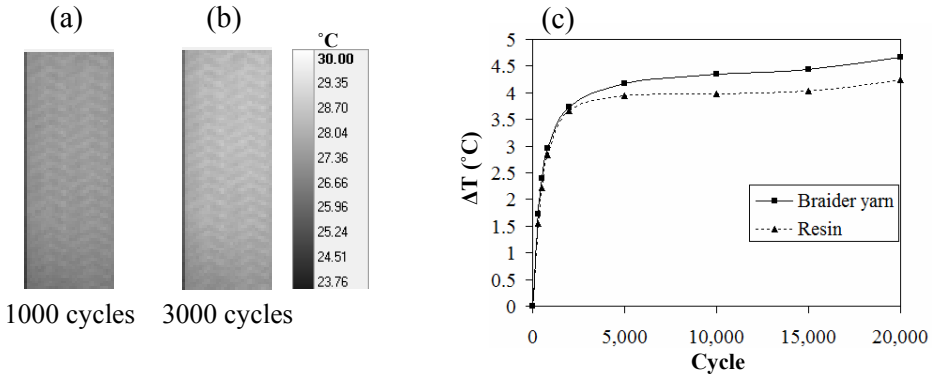

Figure 6. Specimen cycled at 70% UTS: (a)-(b) IRT images, (c) IRT temperature profiles.

Plots of the dynamic stiffness normalized by the static stiffness (E/E_o) are shown in Figure 7 (a) and (b) for the specimens cycled at maximum applied stresses of 70% UTS and 80% UTS, respectively. The stiffness profiles transition from a stage of initial rapid drop to a stage of gradual stiffness degradation. This transition occurs after approximately the same number of cycles that corresponds to the braider yarn crack saturation and the beginning of the temperature plateau for each respective maximum applied stress (e.g., compare Figures 4 (a), 5 (a) and 7 (a)).

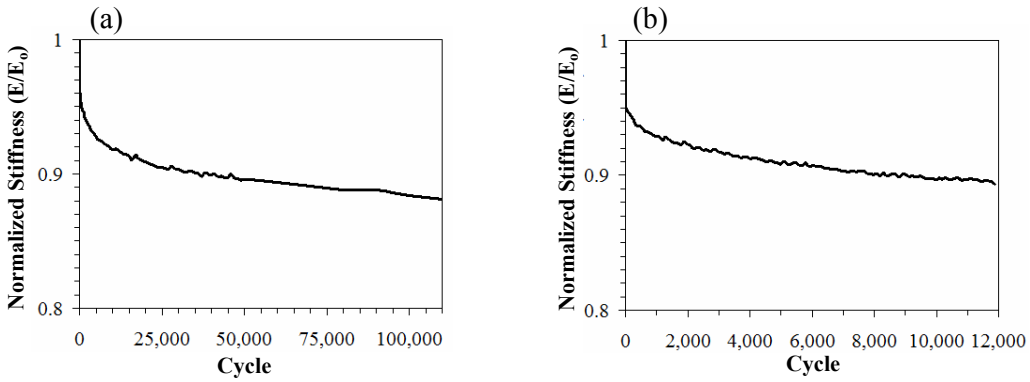

Figure 7. Normalized stiffness profile for test specimens cycled at (a) 70% UTS, and (b) 80% UTS.

4 Discussion

The results obtained through thermographic and mechanical measurements, as well as the qualitative and quantitative data obtained from edge replications provide the basis for this discussion. For the case of tensile static loading, transverse cracks initiated and propagated in the braider yarns along their respective axes (i.e., ±θ) gradually as the applied stress level increased. The cracks began to initiate at low stresses, reaching a much higher density in the latter stages of loading prior to failure. The SEM image analysis confirmed that the braider yarns cracks were in fact the dominant damage mode that ultimately caused failure. These cracks were the main contributors of the higher temperature regions that corresponded to the braider yarns on the surface temperature maps extracted by the IR camera, as was shown in Figure 3. The ability of the IR camera to track the progression of braider yarn cracks was evident by comparing the damage observations made through analysis of the obtained edge replications and *post mortem* SEM images with the specimen surface temperature maps. The fact that the majority of damage was transverse cracking in the braider yarns allows for a conclusion that the IR camera was able to accurately map the damage progression corresponding to quasi-static loading.

For the case of cyclic loading, transverse cracking in the braider yarns was also found to be the dominant damage mechanism for the duration of cycling. Following a rapid initial increase, the braider yarn cracks reached a saturation state in the early stages of cycling for all maximum applied stress levels, which was observed through crack density profiles that were defined using obtained edge replications. Localized interface cracks between adjacent braider yarns were also observed in the early stages of cycling, and were found to increase in length and coalesce with other interface cracks and matrix cracks in the later stages of cycling. The number of interface cracks was significantly less than the number of braider yarn cracks for all tested stress levels. The braider yarn crack saturation state corresponded to the same number of cycles in which the transition of the surface temperature profile reached a plateau. The initial rise in temperature was therefore a result of the initial rapid initiation and propagation of braider yarn cracks and the corresponding crack face friction during cyclic loading, and not mainly due to local viscous heating of the matrix or the initiation of interface cracks. This can in fact be partially attributed to the characteristics of the polyimide matrix which exhibits high thermal stability due to a highly cross-linked molecular structure, which would therefore limit any self-generated viscous heating. Analogous to the static results, the IR images obtained at various cyclic intervals for all cyclic tests revealed that the temperatures in the braider yarns were consistently higher when compared to the resin-rich

zones (see Figure 6). This confirms that the braider yarn cracks are the main contributors to the increase in temperature during cyclic loading.

The stiffness degradation profiles for all cyclic tests transition from a stage of rapid degradation to more gradual degradation. This transition occurs after the same number of cycles that the braider yarn cracks saturate. It can therefore be concluded that the braider yarn crack initiation and propagation is the main cause of the initial rapid stiffness degradation, which was also detected by the IR camera through the temperature-cycle profile. After braider yarn crack saturation, the stiffness continued to degrade at a gradual rate, which was due to the propagation of the existing interface cracks. The braider yarns would tend to rotate slightly towards the loading direction, which would increase the shear stresses at the braider yarn crossover locations and propagate the interface cracks. This however did not cause any notable increase in temperature, which is expected since the propagation of these cracks is gradual as observed through edge replications.

5 Conclusion

The relation between fatigue damage development in terms of braider yarn crack density and stiffness degradation for the investigated braided polymeric composite material was established. The use of infrared thermographs to predict material property degradation and to monitor the underlying damage mechanisms causing degradation (i.e., braider yarn cracks) was shown. The thermographs were capable of establishing local high temperature regions that corresponded to damage within the braider yarns. The temperature profiles were correlated with the saturation of braider yarn cracks and the stiffness degradation behaviour during cyclic loading. Although additional testing is required to further validate the usefulness of thermography for damage monitoring and for predicting the onset of critical damage states, the obtained results provide further support for infrared thermography as a viable non-destructive evaluation tool for testing of textile polymeric composite materials. This is important for the development and design of components manufactured from these advanced materials. Infrared thermography can be compared to another full-field non-destructive evaluation technique such as x-ray tomography to further confirm the findings of this study. In additional ongoing work, the use of this technique on other textile composite components may further reveal the usefulness of this method for assessing critical damage states and also for predicting failure locations under cyclic loading.

References

[1] Bourchak M., Farrow I.R., Bond I.P., Rowland C.W., Menan F. Acoustic emission energy as a fatigue damage parameter for CFRP composites. *International Journal of Fatigue*, **29**, pp. 457-470 (2007).

[2] Beghini, M., Bertini, L., Vitale, E. Analysis of fatigue delamination growth in carboresin specimens with central hole. *Composite Structures*, **17**, pp. 257-274 (1991).

[3] Bathias C., Cagnasso A. *Application of X-ray Tomography to the Non-destructive Testing of High-performance Polymer Composites* in "Damage Detection in Composite Materials", edited by Masters J.E. ASTM International, Philadelphia, **STP 1128**, pp. 35-54 (1992).

[4] Steinberger R., Valadas-Leitao T.I., Ladstatter E., Pinter G., Billinger W., Lang R.W. Infrared thermographic techniques for non-destructive damage characterization of carbon fibre reinforced polymers during tensile fatigue testing. *International Journal of Fatigue*, **28**, pp. 1340-1347 (2006).

[5] Toubal L., Karama M., Lorrain B. Damage evolution and infrared thermography in woven composite laminates under fatigue loading. *International Journal of Fatigue*, **28**, pp. 1867-1872 (2006).
[6] Masters, J.E., Ifju, P.G. A phenomenological study of triaxially braided textile composites loaded in tension. *Composites Science and Technology*, **56**, pp. 347-358 (1996).
[7] Bremond, P. *Lock-in thermography: A tool to measure stress and to detect defects in aircraft industry* in "Proceedings of *9th Australian International Aerospace Congress*", Canberra, Australia (2001).